ISSN 0023-1584, Kinetics and Catalysis, 2009, Vol. 50, No. 3, pp. 456–460. © Pleiades Publishing, Ltd., 2009.
Original Russian Text © E.A. Mel'gunova, A.N. Shmakov, Yu.V. Larichev, M.S. Mel'gunov, 2009, published in Kinetika i Kataliz, 2009, Vol. 50, No. 3, pp. 476–480.

# Effect of the Concentration of Aluminum on the Adsorption, Texture, and Structure Characteristics of a Mesoporous Mineral Mesophase of the SBA-15 Type

**E. A. Mel'gunova, A. N. Shmakov, Yu. V. Larichev, and M. S. Mel'gunov**

*Boreskov Institute of Catalysis, Siberian Branch, Russian Academy of Sciences, Novosibirsk, 630090 Russia*
*e-mail: larichev@catalysis.ru*

Received October 12, 2007

**Abstract**—The effect of Al ion implantation on the properties of mesoporous aluminosilicate mineral phases of the SBA-15 type was studied. The implantation of Al was performed immediately under conditions of the synthesis of SBA-15 in a weakly acidic medium (pH ~ 2.9). It was found that, under these conditions, the amount of Al that can be implanted into the SBA-15 framework is limited (a maximum of 7.2 mol %). According to XPS data, aluminum ions were implanted into the matrix of silica rather than occurring on the surface as an individual phase. The study of nitrogen adsorption at 77 K and the results obtained by X-ray diffractometry and high-resolution electron microscopy suggest that Al–SBA-15 materials exhibited a hexagonal structure of channel pores of the same diameter of 8.3 nm, and the unit cell parameter was 12.3 nm. The degree of crystallinity of the material increased with the concentration of Al.

**DOI:** 10.1134/S0023158409030185

## INTRODUCTION

Silicate materials of the SBA-15 type [1] belong to a family of new mesoporous solid-phase materials, which are structurally similar to liquid crystals; that is, they exhibit a long-range order (3 nm or more) in the absence of a short-range (atomic) order. Because of this structure peculiarity, we will use the term mesophases in this work to designate these materials. Mesophases of the SBA-15 type are characterized by a hexagonal packing of cylindrical channel pores with a narrow pore-diameter distribution; they are prepared with the use of the nonionic surfactant Pluronic P123. The average pore diameter depends on synthesis conditions, and it can vary from 5 to 10 nm. The length of channels depends on the longitudinal size of mesophase particles, and it can be as great as 500 nm. The channels are separated by porous walls of amorphous $SiO_2$ about 2.0 nm in thickness. These materials exhibit high hydrothermal stability; by analogy with microporous zeolites, they can be considered as promising adsorbents and catalysts.

Two procedures are in current use for the implantation of active catalytic centers into the silicate framework of SBA-15; they differ in the steps at which the implantation is performed. The first procedure (post synthesis) is based on the introduction of the elements (Al, Ti, etc.) into a preformed mesophase [2–5]. The disadvantages of this version are the sophisticated synthetic procedure (especially for V and Ti) and the possibility of the deposition of additives as individual phases both within mesopores and on the outer surface of the mesophase; this can adversely affect the catalytic and adsorption properties of the materials. The second procedure (direct synthesis) consists in the coprecipitation of additives and $SiO_2$ immediately in the course of the mesophase synthesis [6, 7]. However, up to now, it has been impossible to obtain mesophases with a satisfactory degree of crystallinity under known synthesis conditions at $1.5 < pH < 4.0$. At the same time, the above range of pH should be considered as the most appropriate for the synthesis of catalytic systems based on Al–, Zr–, and Ti–silicate mesophases. Mel'gunov et al. [8] reported previously on the synthesis of Al–SBA-15 in a moderate acidity region ($2.6 < pH < 3.1$). In this work, we consider the results of a study on the adsorption, texture, and structure properties of these materials.

## EXPERIMENTAL

The series of mesophase samples of the Al–SBA-15 type with various concentrations of Al cations was synthesized by the interaction of a soluble form of $SiO_2$ with the surface-active poly(ethylene oxide)-poly(propylene oxide)-poly(ethylene oxide) triblock copolymer $(EO)_{20}(PO)_{70}(EO)_{20}$ (trade name: Pluronic P123, henceforth referred to as P123) at the molar ratio $[P123] : [Al((SO)_4)_3] : [SiO_2] : [NaOH] : [HCl] : [H_2O] = 1 : X : 3 : 3 : 3 : (30 + 0.1X)$ $(0.01 < X < 0.18)$. For this purpose, an aqueous solution of P123 with $Al((SO)_4)_3$ and an aqueous solution of $Na_2Si_2O_5$ were prepared separately. The solutions were mixed with a magnetic stirrer, and the resulting white precipitate was allowed

to stand for 50 h at room temperature. Thereafter, the mixture was treated in an autoclave at 383 K for 50 h. In the course of the synthesis, HCl was added to the mixture to adjust the required value of pH in the solution. Then, the resulting samples were numbered from 1 to 11. The greater the number, the higher the concentration of $Al((SO)_4)_3$ in the synthetic mixture.

The X-ray diffraction patterns were measured on a diffractometer using synchrotron radiation (wavelength of 0.154 nm) in accordance with a specially developed procedure for measurements in the region of very small angles. The samples were in an air-dry state; the measurements were performed in the region of 2θ angles from 0.5° to 7° with a step of 0.02° at an accumulation time of 20 s at each point. To provide high instrumental resolution, a perfect Ge(111) flat analyzing crystal and a plane-parallel collimator, which restricted the azimuthal divergence of the diffracted beam to 5 mrad, were used. Because of this, the instrumental broadening of reflections in the angle region of 2θ from 1° to 7° was no greater than 0.04°, and the unit cell parameters were calculated to within ±0.02 nm. The cell parameters were calculated based on the {10} reflection with the use of the Selyakov–Scherrer equation.

The adsorption characteristics of the materials were determined on a Micromeritics ASAP 2400 system using a standard procedure of nitrogen adsorption at 77 K after sample evacuation at 500 K for 12–16 h to a residual pressure of lower than $10^{-3}$ Torr. A comparative method [9, 10] was used to calculate texture parameters. The mesopore size distribution was found by analyzing the desorption branches of isotherms using the Barrett–Joiner–Halenda method [11].

The mesophase images were obtained on a JEM-100CX transmission electron microscope.

XPS spectra were recorded on a VG ESCALAB HP electron spectrometer with the use of unmonochromated Al$K_\alpha$ radiation ($h\nu$ = 1486.6 eV; 200 W). Both survey XPS spectra and their narrow regions characteristic of the main components of mesophase materials—silicon (Si 2*p*), aluminum (Al 2*p*), oxygen (O 1*s*), and carbon (C 1*s*)—were analyzed. Lines due to other impurity elements were not detected in the samples. The survey spectra were recorded at an analyzer transmission energy of 50 eV, and the spectra of particular regions were recorded at 20 eV (in order to increase the energy resolution). The binding energy ($E_b$) scale was precalibrated using the peak positions of the Au $4f_{7/2}$ (84.0 eV) and Cu $2p_{3/2}$ (932.6 eV) core levels. The accuracy of the determination of $E_b$ was ±0.1 eV. The samples were supported onto a conducting substrate and studied with no pretreatment. An internal standard technique was used to take into consideration charging in the samples based on the C 1*s* (284.9 eV) and Si 2*p* (104.0 eV) lines. The relative concentrations of the elements on the surfaces of the samples expressed as atomic concentration ratios were calculated from the integrated intensities of corresponding photoelectron lines with consideration for atomic sensitivity factors [12]:

$$n_x = \frac{I_x/\mathrm{ASF}_x}{I_\mathrm{C}/\mathrm{ASF}_\mathrm{C}},$$

where $n_x$ is the ratio between the surface concentrations (in at %) of the elements $x$ and C in the analysis zone; $I_x$ and $I_\mathrm{C}$ are the line intensities of the elements $x$ and C, respectively; and $\mathrm{ASF}_x$ and $\mathrm{ASF}_\mathrm{C}$ are the atomic sensitivity factors of the specified elements, respectively. The measured binding energies were compared with the values of $E_b$ for the reference samples of γ-$Al_2O_3$ and $SiO_2$.

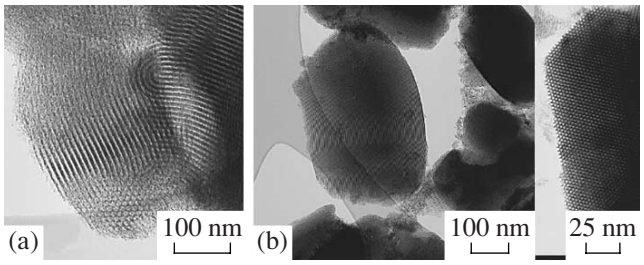


**Fig. 1.** Electron micrographs of samples (a) 1 (Al/Si = 0.009) and (b) 11 (Al/Si = 0.072).

## RESULTS AND DISCUSSION

Figure 1 shows the electron micrographs of samples 1 and 11. Sample 1 consisted of domains with different sizes (from 10 to 300 nm); pores in these domains were strongly curved, although they exhibited an apparent spatial orientation. The pore diameter can be estimated at 7–8 nm; the distance between the axes of neighboring channels was about 10.6 nm, whereas the wall thickness between the channels was 2.5–3.5 nm. Sample 11 consisted of more uniform particles of sizes from 0.30 to 1.5 μm. Pores formed almost rectilinear parallel channels, whose length was commensurable with the particle size; this length can be as great as 1.5 μm. Figure 1b shows two micrographs with different magnifications. The rectilinear parallel channels can be most clearly seen in the micrograph with a greater magnification. The pore diameter and the distance between the axes of neighboring channels were the same as those in sample 1.

Figure 2 shows the diffraction patterns of samples 1 and 11. The former exhibits four reflections ({10}, {11}, {20}, and {21}), which suggest a two-dimensional hexagonal organization of pores in the mesophase. Reflections in the diffraction pattern of sample 11 also correspond to a two-dimensional hexagonal packing; however, they are more intense. In addition, the clearly pronounced reflection {30} is observed in this case.

Thus, the results obtained using synchrotron radiation diffraction and transmission electron microscopy

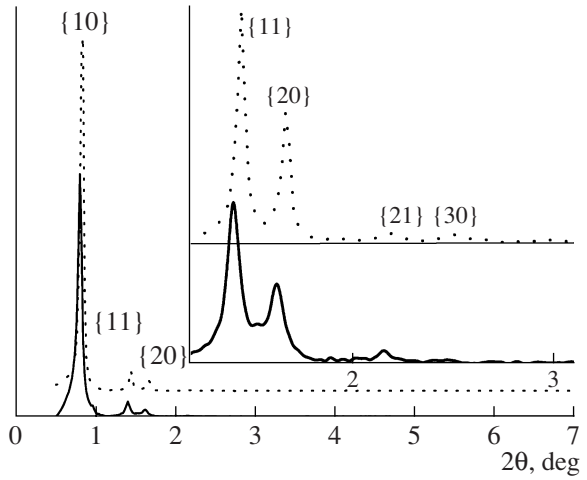


**Fig. 2.** X-ray diffraction patterns of samples (solid line) 1 (Al/Si = 0.009) and (dotted line) 11 (Al/Si = 0.072). Insert: scaled-up fragments of the X-ray diffraction patterns. Corresponding reflections are specified in curly brackets.

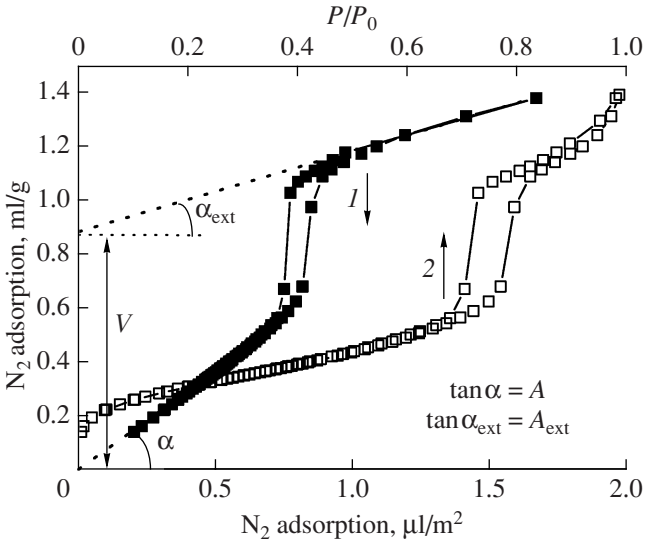


**Fig. 3.** Isotherms of nitrogen adsorption at 77 K on sample 11 in (*1*) standard and (*2*) comparative coordinates. The volume of adsorbed $N_2$ is specified in terms of the liquid state.

indicated that the test samples consisted of particles with a two-dimensional hexagonally ordered structure of channel pores. In this case, the degree of crystallinity considerably increased with the concentration of Al in the mixture. According to structure data, the unit cell parameter decreased as the concentration of Al was increased. The unit cell parameters of samples 1 (Al/Si = 0.009) and 11 (Al/Si = 0.072) were 12.7 and 12.3 nm, respectively.

Figure 3 shows the adsorption–desorption isotherm of nitrogen on sample 11 at 77 K in standard and comparative coordinates. The shapes of isotherms for the other samples were analogous; therefore, these isotherms are not given here. Table 1 summarizes the channel pore volumes ($V$), the total specific surface areas ($A$), and the external surface areas of mesophase particles ($A_{ext}$), as found by a comparative method. In the region of small surface coverages, straight lines in the comparative coordinates are practically extrapolated to the zero point in the axis of ordinates for all of the samples. This fact suggests the absence of micropores from mesophase channel walls. An increase in the concentration of Al was accompanied by an insignificant increase (by ~10%) in the total specific surface area of the sample. In this case, changes in $V$ and $A_{ext}$ exhibited an extremal character. For example,

**Table 1.** Texture characteristics of the materials

| Sample no. | Al/Si | | Specific surface area, $m^2/g$ | | Pore volume, $cm^3/g$ | Average pore diameter, nm | $w$*, nm |
|---|---|---|---|---|---|---|---|
| | in the mixture during the synthesis | according to elemental analysis data | total | external | | | |
| 1 | 0.009 | 0.009 | 687 | 380 | 0.90 | 7.58 | 0.93 |
| 2 | 0.018 | – | 655 | 370 | 0.81 | 7.44 | 0.80 |
| 3 | 0.036 | 0.031 | 666 | 391 | 0.83 | 7.43 | 0.74 |
| 4 | 0.054 | – | 680 | 453 | 0.78 | 7.35 | 0.77 |
| 5 | 0.072 | 0.050 | 677 | 413 | 0.69 | 7.15 | 0.72 |
| 6 | 0.090 | – | 752 | 455 | 0.68 | 6.84 | 0.74 |
| 7 | 0.108 | 0.074 | 726 | 446 | 0.65 | 6.79 | 0.56 |
| 8 | 0.126 | – | 716 | 385 | 0.75 | 7.14 | 0.69 |
| 9 | 0.144 | 0.067 | 734 | 388 | 0.74 | 7.07 | 0.69 |
| 10 | 0.162 | – | 741 | 353 | 0.80 | 7.05 | 0.68 |
| 11 | 0.180 | 0.072 | 741 | 303 | 0.87 | 7.10 | 0.64 |

* Halfwidth of the peak of a pore-size distribution in an interpolation using the Gauss equation.

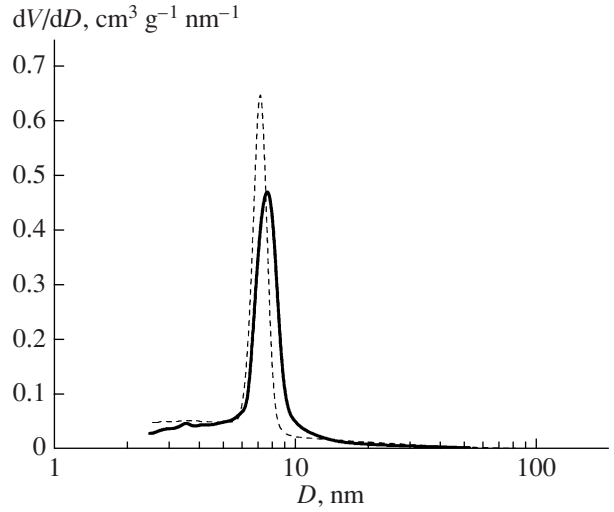


**Fig. 4.** Mesopore size distribution in samples 1 (dashed line) 1 and 11 (solid line). *D* is the pore diameter.

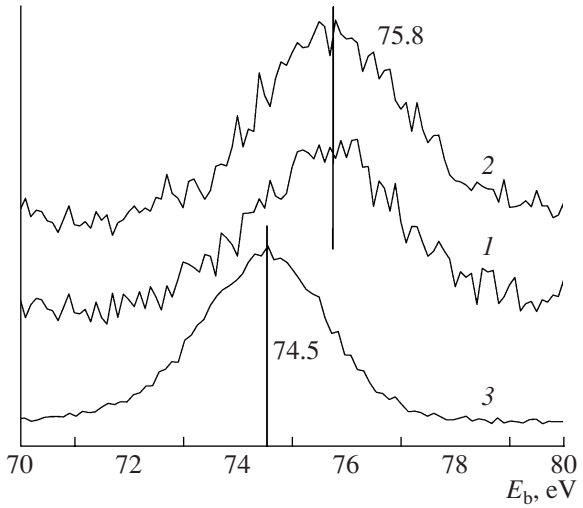


**Fig. 5.** Al 2*p* XPS spectra of samples (*1*) 7 (Al/Si = 0.074), (*2*) 11 (Al/Si = 0.072), and (*3*) γ-$Al_2O_3$.

a 28% decrease in the pore volume of sample 7, as compared with sample 1, corresponded to a 20% increase in the external surface area of mesophase particles. An increase in the external surface area of particles is indirect evidence of a decrease in the average size of mesophase particles.

Figure 4 shows mesopore size distributions in samples 1 and 11, as calculated from the desorption branches of the isotherms of nitrogen adsorption at 77 K. The other samples exhibited analogous distributions, which are not given here. As can be seen in Fig. 4, the main distribution peak shifted toward a smaller diameter (from 7.6 to 7.1 nm) as the amount of implanted Al was increased; in this case, the peak width decreased. The average channel-pore diameter in the starting SBA-15 mesophase (without Al) was 7.6 nm.

It was of interest to determine the nature of aluminum added to silicate mesophases, namely, to find out whether Al ions were fully embedded in the silicate matrix structure or whether they occurred partially as an individual X-ray amorphous phase of aluminum sulfate or oxide.

Within the limits of the sensitivity of XPS, we did not detect S 2*p* signals; this fact suggests the absence of the starting aluminum sulfate from the samples. The samples with low aluminum concentrations were not analyzed because of the low intensity of the Al 2*p* signal. No considerable difference between samples 7 and 11 was detected, although the rated concentrations of aluminum in the synthetic mixtures were different. Table 2 summarizes binding energies in both test samples and reference samples. The O 1*s* and Si 2*p* binding energies for samples 7 and 11 coincided with the corresponding values for $SiO_2$. At the same time, the Al 2*p* binding energy in samples 7 and 11 was much greater (by 1.2–1.3 eV) than that in the reference sample of γ-$Al_2O_3$ (Fig. 5). This fact suggests that aluminum ions in samples 7 and 11 had a stronger acceptor environment, as compared with that in aluminum oxide. Such increased Al 2*p* binding energies are also characteristic of zeolites, in which aluminum ions are inserted into the zeolite crystal structure [13]. This allowed us to conclude that aluminum ions were inserted into the matrix of silicon oxide rather than occurring as an X-ray amorphous phase of aluminum oxide on the surface of silica. Comparing the Al/Si ratios in samples 7 and 11 found by elemental analysis and XPS (Tables 1, 2), note that the aluminum concentrations on the surfaces of these samples were much lower than the bulk concentrations; that is, aluminum ions were nonuniformly distributed in the silicate matrix.

Thus, in this work, we studied the effect of the implantation of aluminum ions on the properties of mesoporous aluminosilicate mineral mesophases of the SBA-15 type. We found that the amount of Al that could be implanted into the SBA-15 framework under the conditions used was limited (a maximum of 7.2 mol %). Aluminum ions were embedded in the silicon oxide matrix rather than occurring as an individual X-ray amorphous phase of alumina on the surface. The Al–SBA-15 materials exhibited a hexagonal structure

**Table 2.** Si 2*p*, Al 2*p*, and O 1*s* binding energies and Al/Si atomic ratios in the test samples and the reference samples of $SiO_2$ and γ-$Al_2O_3$

| Sample | $E_b$, eV | | | Al/Si |
|---|---|---|---|---|
| | Si 2*p* | Al 2*p* | O 1*s* | |
| 7 (Al/Si = 0.074) | 104.0 | 75.7 | 533.3 | 0.050 |
| 11 (Al/Si = 0.072) | 104.0 | 75.8 | 533.3 | 0.058 |
| $SiO_2$ | 104.0 | – | 533.3 | – |
| γ-$Al_2O_3$ | – | 74.5 | 531.4 | – |

of channel pores with uniform diameters of 7–8 nm; the unit cell parameter was 12.3 nm. The degree of crystallinity of the material increased with the concentration of Al.

## ACKNOWLEDGMENTS

This work was supported by the Russian Foundation for Basic Research (project no. 06-03-32268-a).

## REFERENCES

1. Zhao, D., Feng, J., Huo, Q., Melosh, N., Fredricson, G.H., Chmelka, B.F., and Stucky, J.D., *Science*, 1998, vol. 279, p. 548.
2. Luan, Z., Hartmann, M., Zhao, D., Zhou, W., and Kevan, L., *Chem. Mater.*, 1999, vol. 11, p. 1621.
3. Zeng, S., Vlanshard, J., Vreusse, M., Shu, I.X., Nie, H., and Li, D., *Microporous Mesoporous Mater.*, 2005, vol. 85, p. 297.
4. Mokaya, R. and Jones, W., *Chem. Commun.*, 1998, p. 1839.
5. Oumi, Y., Takagi, H., Sumiya, S., Mizuno, R., Uozumi, T., and Sano, T., *Microporous Mesoporous Mater.*, 2001, vols. 44–45, p. 267.
6. Yue, Y., Gedeon, A., Bonardet, J.-L., Melosh, N., D'Espinose, J.-B., and Fraissard, J., *Chem. Commun.*, 1999, p. 1697.
7. Zheng, Y., Li, J., Zhao, N., Wei, W., and Sun, Y., *Microporous Mesoporous Mater.*, 2006, vol. 92, p. 195.
8. Mel'gunov, M.S., Mel'gunova, E.A., Shmakov, A.N., and Zaikovskii, V.I., *Stud. Surf. Sci. Catal.*, 2003, vol. 146, p. 543.
9. Karnaukhov, A.P., Fenelonov, V.B., and Gavrilov, V.Yu., *Pure Appl. Chem.*, 1989, vol. 61, p. 1913.
10. Fenelonov, V.B., Romannikov, V.N., and Derevyankin, A.Yu., *Microporous Mesoporous Mater.*, 1999, vol. 28, p. 57.
11. Barrett, E.P., Joyner, L.G., and Halenda, P.H., *J. Am. Chem. Soc.*, 1951, vol. 73, p. 373.
12. Moulder, J.F., Stickle, W.F., Sobol, P.E., and Bomben, K.D., *Handbook of X-ray Photoelectron Spectroscopy*, Eden Prairie, Minn.: PerkinElmer, 1992.
13. Barr, T.L., *Appl. Surf. Sci.*, 1983, vol. 15, p. 1.